THE ROYAL SOCIETY

doi 10.1098/rspb.2000.1396

A three-dimensional model for ciliary motion based on the internal 9 + 2 structure

Shay Gueron[1*] **and Konstantin Levit-Gurevich**[2]

[1]*Department of Mathematics, University of Haifa, Haifa, 31905, Israel*
[2]*Department of Mathematics, Technion–Israel Institute of Technology, Haifa, 32000, Israel*

Here we present, to our knowledge, the first modelling platform that enables simulations of three-dimensional (3D) motion of multicilia arrays at a detailed level. It consists of three building blocks: (i) geometric equations for tracking the 3D motion of the cilia, (ii) a hydrodynamic description of the ciliary system, and (iii) model equations for the internal bend generating based on the $9 + 2$ structure. The model generates seemingly realistic 3D beat patterns and demonstrates metachronal coordination that evolves autonomously as a result of the hydrodynamic coupling between the cilia. We study the effect of the twisting motion within the cilia and propose a conjecture on a possible role of the radial spokes system.

Keywords: ciliary motion; three-dimensional motion; slender rods

1. INTRODUCTION

Cilia and flagella are tiny hair-like cell appendices. They are responsible for many essential biological functions in the respiratory, digestive and reproductive systems and for micro-organisms' locomotion and feeding. Their study is important in biology and medicine and has attracted a great deal of research effort for some 250 years. Theoretical research in this area is mainly orientated towards understanding how the ciliary internal structure produces the complex motion we see, how it is controlled, how it responds to external load and how cilia synchronize with their neighbouring cilia (Hines & Blum 1978; Gueron & Liron 1992, 1993; Murase 1992; Gueron & Levit-Gurevich 1998, 1999).

Typically, ciliary beat patterns consist of two phases: (i) the effective stroke, where a cilium moves approximately as a straight rod, and (ii) the recovery stroke, where it bends and rolls back to its original initial state. Metachronal coordination between cilia is a situation where large numbers of cilia beat together with a constant phase difference between adjacent neighbours, their tips forming a moving wave pattern. The reason why and how arrays of cilia beat in a metachronal pattern is not understood. Membrane voltage and calcium levels may affect the direction of the metachronal wave and also the directions of the effective and recovery strokes (Machemer 1972). It has also been proposed that the metachronism phenomenon may be the result of hydrodynamical coupling between the cilia through the viscous fluid (Sleigh 1974; Gheber & Priel 1989). Our work has, to our knowledge, provided the first theoretical model that supports this conjecture. In Gueron *et al.* (1997) we developed a model which treats a cilium as a slender body in order to describe the motion of the cilium within the flow field generated by all other cilia, given the cilium's 'internal engine'. We constructed an 'internal motor' in order to mimic the motion of a single cilium of the ciliated protozoan *Paramecium*. To avoid hypothesizing a biologically unmotivated internal clock we used a geometric switch hypothesis—a switching mechanism that governs the transition from effective to recovery stroke and back, based on the configuration of the cilium (see also Gueron & Levit-Gurevich 1998). Simulating single- and multicilia configurations led to results surprisingly consistent with experimental observations: beat frequency decayed logarithmically with increased fluid viscosity, two adjacent cilia initially out of phase phase-locked within a few cycles and arrays of cilia performed coordinated beats resembling metachronal waves. In Gueron & Levit-Gurevich (1999) we computed the energy consumption of a cilium during its beat cycle which reflects an existing paradigm on the basics of the mechanochemical cycle.

All of these results were obtained for cilia having planar beats, but some research was also directed towards three-dimensional (3D) ciliary beating. Here we mention a few related references, namely Hines & Blum (1983), Sugino & Machemer (1987, 1988), Mogami *et al.* (1992), Gueron & Liron (1993), Teunis & Machemer (1994) and Wooley & Vernon (1999).

In this report we extend our research to 3D beats, which are shown by most real cilia. We present the first modelling platform for simulations of 3D motion of multicilia arrays at a detailed level that accounts for the $9 + 2$ internal structure.

2. A COMPLETE MODELLING FRAMEWORK FOR SIMULATING THREE-DIMENSIONAL CILIARY MOTION

(a) *The body coordinate system*

We consider the model cilium as an inextensible elastic cylindrical sheath of radius a and centre line $\boldsymbol{r}(s,t) = (x(s,t)), y(s,t)), z(s,t))$, where $0 \leqslant s \leqslant 1$ is the arc-length parameter, t is time and the representation is related to some fixed coordinate system whose axes are x, y and z. At each point $A(s,t) = (x(s,t)), y(s,t)), z(s,t))$ along the inextensible centre line, the normal plane $\Pi(s,t)$ is the plane passing through $A(s,t)$ and perpendicular to the tangent direction to $\boldsymbol{r}(s,t)$. We assume that, for all $0 \leqslant s \leqslant 1$ and $t \geqslant 0$, the ciliary cross-section remains

*Author for correspondence (shay@math.haifa.ac.il).

Received 8 June 2000 *Accepted* 6 November 2000

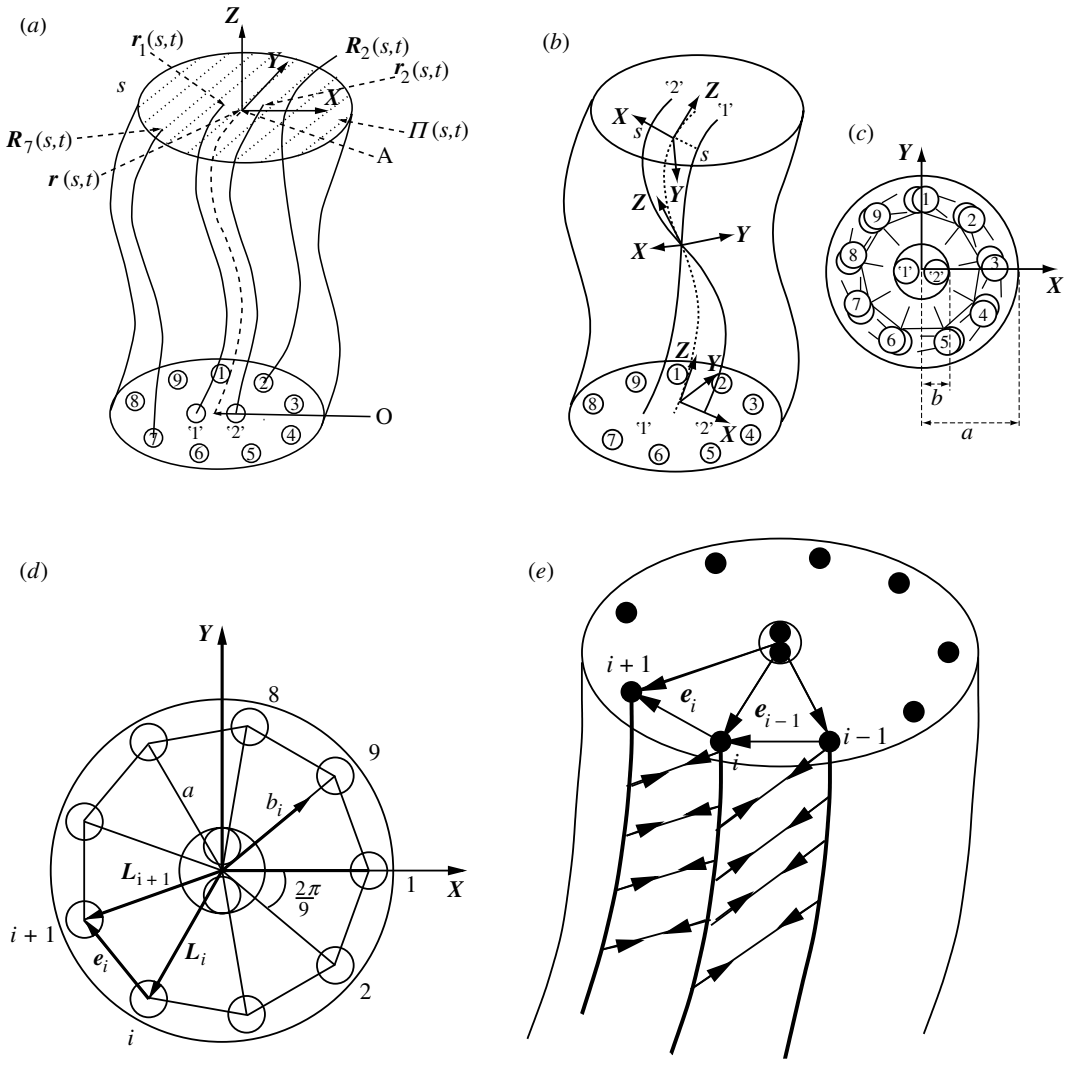

Figure 1. A schematic representation of the body coordinate system of cilium. (*a*) Bent, untwisted cilium, (*b*) twisted and bent cilium, (*c*) the body coordinates at the cross-section, (*d*) the geometric description of the cross-section, and (*e*) filament interconnection due to attached dynein arms.

planar and circular and, therefore, lies in $\Pi(s,t)$. At each point along $\boldsymbol{r}$, we define an orthonormal right-handed coordinate system called *body coordinates* which is defined by the three unit vectors $\boldsymbol{X}=\boldsymbol{X}(s,t)$, $\boldsymbol{Y}=\boldsymbol{Y}(s,t)$ and $\boldsymbol{Z}=\boldsymbol{Z}(s,t)$. The unit vector $\boldsymbol{Z}$ points in the direction of the tangent and $\boldsymbol{X}$ and $\boldsymbol{Y}$ lie in the plane $\Pi(s,t)$ (see figure 1*a*). To define $\boldsymbol{X}$, we observe the two filaments of the central pair, denoted by $\boldsymbol{r}_1(s,t)$, $\boldsymbol{r}_2(s,t)$. At $s=0$, the central pair filaments are located symmetrically at a distance b from the centre line. We assume that $b/a \ll 1$, which is reasonable in our context (e.g. for the cilium of *Paramecium* $b/a \approx 0.15$–0.2) (see Sleigh 1962). At a distance $\approx a$ from the centre we have the nine doublets (microtubule filaments) denoted by $\boldsymbol{R}_1(s,t))$, $\boldsymbol{R}_2(s,t))$, $\ldots$, $\boldsymbol{R}_9(s,t)$ arranged symmetrically around at the centre line. These 11 filaments are connected to each other by dynein arms, nexin links and radial spokes. Since $b/a \ll 1$ we assume that $\Pi(s,t)$ contains the end-points of $\boldsymbol{r}_1$ and $\boldsymbol{r}_2$ and define the X-axis as the unit vector pointing in the direction of the line connecting the end-points of $\boldsymbol{r}_1$ and $\boldsymbol{r}_2$ (which also passes through the corresponding end-point of $\boldsymbol{r}$). The $\mathcal{Y}$-axis is defined by $\boldsymbol{Y}=\boldsymbol{Z}\times\boldsymbol{X}$ (for a right-handed system). This body coordinate system is shown schematically in figure 1*a–c*.

Here we shall use the following convention. The subscripts X, $\mathcal{Y}$ and $\mathcal{Z}$ denote the components of vectors in the body coordinate system, the subscript s denotes differentiation with respect to s and the superscript dot denotes differentiation with respect to t.

The centre line moves at velocity $\boldsymbol{V}=\boldsymbol{V}(s,t)$ and rotates (with the whole cross-section) about its longitudinal axis $\boldsymbol{Z}(s,t)$ at angular velocity $\boldsymbol{\Omega}=\boldsymbol{\Omega}(s,t)$ $=\boldsymbol{\Omega}(s,t)\,\boldsymbol{Z}(s,t)$.

(b) *The curvature in body coordinates*

The unit vectors $\boldsymbol{X}(s,t)$, $\boldsymbol{Y}(s,t)$ and $\boldsymbol{Z}(s,t)$ change as a function of s at rates we denote by $\kappa_X=\kappa_X(s,t)$ and $\kappa_{\mathcal{Y}}=\kappa_{\mathcal{Y}}(s,t)$ and $\kappa_{\mathcal{Z}}=\kappa_{\mathcal{Z}}(s,t)$, respectively. These rates have the following geometric interpretation: if the infinitesimal change from body coordinates at s to body coordinates at $s+\mathrm{d}s$ is represented as successive rotations by the angles $\theta_X=\theta_X(s,t)$, $\theta_{\mathcal{Y}}=\theta_{\mathcal{Y}}(s,t)$ and $\theta_{\mathcal{Z}}=\theta_{\mathcal{Z}}(s,t)$ about the X-, $\mathcal{Y}$- and $\mathcal{Z}$-axes, respectively, then $\kappa_X=\partial\theta_X/\partial s$, $\kappa_{\mathcal{Y}}=\partial\theta_{\mathcal{Y}}/\partial s$ and $\kappa_{\mathcal{Z}}=\partial\theta_{\mathcal{Z}}/\partial s$. Thus, κ_X and $\kappa_{\mathcal{Y}}$

represent rotation about the X- and Y-axes (in the Y–Z and X–Z planes), respectively, and κ_Z represents rotation about the Z-axis, i.e. a longitudinal twist. We define $\boldsymbol{\kappa} = \boldsymbol{\kappa}(s,t) = (\kappa_X, \kappa_Y, \kappa_Z)$. The centre line's curvature is $\kappa = \sqrt{\kappa_X^2 + \kappa_Y^2}$ and, if $\kappa \neq 0$, the torsion is $\tau = -\kappa_Z - (\kappa_X \kappa_{Y_s} - \kappa_{X_s}\kappa_Y)/\kappa^2$ (see Gueron & Liron (1993) for details).

It can be shown that there exists a unique vector $\boldsymbol{\omega} = (\omega_X(s,t)), \omega_Y(s,t)), \omega_Z(s,t))$ such that differentiation with respect to t of an arbitrary vector $\boldsymbol{u} = \boldsymbol{u}(s,t)$ is expressed by $\dot{\boldsymbol{u}} = (\dot{\boldsymbol{u}})_{\text{body}} + \boldsymbol{\omega} \times \boldsymbol{u}$ in the body coordinate system. The components $\boldsymbol{\omega} = (\omega_X(s,t), \omega_Y(s,t)), \omega_Z(s,t))$ describe the rates of change (in time) of the orientation of the unit vectors $\boldsymbol{X}(s,t)$, $\boldsymbol{Y}(s,t)$ and $\boldsymbol{Z}(s,t)$. Note that $\omega_Z(s,t)$ is *not* equal to the angular velocity $\Omega(s,t)$ and an appropriate relationship between these quantities appears in proposition 1.

(c) *The three components of the dynamic model*

(i) *Geometric equations for the dynamics of a 3D inextensible filament as a function of a given velocity distribution along its centre line*

To track the dynamics of a 3D rod we use a newly developed system of partial differential equations, which is valuable in a variety of other contexts as well. The (lengthy) derivation is detailed in Gueron & Levit-Gurevich (2000).

Proposition 1

Let $\boldsymbol{r}(s,t)$, $0 \leqslant s \leqslant 1$, be an inextensible curve of length 1, moving in space at velocity $\boldsymbol{V} = \boldsymbol{V}(s,t)$ and rotating at angular velocity $\boldsymbol{\Omega} = \boldsymbol{\Omega}(s,t)\boldsymbol{Z}(s,t)$. The time-evolution of its local coordinates curvature is determined by the following equations:

$$\begin{aligned}\dot{\kappa}_X = {} & \kappa_Y\omega_Z - V_{Y_{ss}} - 2\kappa_Z V_{X_s} + 2\kappa_X V_{Z_s} - \kappa_{Z_s} V_X \\ & + \kappa_{X_s} V_Z - \kappa_X\kappa_Y V_X + (\kappa_X^2 + \kappa_Z^2) V_Y - \kappa_Y\kappa_Z V_Z, \quad (1)\end{aligned}$$

$$\begin{aligned}\dot{\kappa}_Y = {} & -\kappa_X\omega_Z + V_{X_{ss}} - 2\kappa_Z V_{Y_s} + 2\kappa_Y V_{Z_s} - \kappa_{Z_s} V_Y \\ & + \kappa_{Y_s} V_Z + \kappa_X\kappa_Y V_Y - (\kappa_Y^2 + \kappa_Z^2) V_X + \kappa_X\kappa_Z V_Z, \quad (2)\end{aligned}$$

$$\dot{\kappa}_Z = \omega_{Z_s} + \kappa_X(V_{X_s} - \kappa_Z V_Y) + \kappa_Y(V_{Y_s} + \kappa_Z V_X), \quad (3)$$

$$\omega_{Z_s} = \Omega_s - \kappa_X(V_{X_s} - \kappa_Z V_Y) - \kappa_Y(V_{Y_s} + \kappa_Z V_X). \quad (4)$$

Inextensibility, i.e. no velocity changes occurring along the centre line in the tangent direction, imply

$$\boldsymbol{Z} \times \boldsymbol{V}_s = V_{Z_s} - \kappa_Y V_X + \kappa_X V_Y = 0. \quad (5)$$

Thus, the motion of the inextensible curve is determined by the velocity components V_X and V_Y and the twisting velocity $\boldsymbol{\Omega}$.

Reconstructing $\boldsymbol{r}$ from κ_X, κ_Y and κ_Z, suppose that κ_X, κ_Y and κ_Z are known at some time t_0, as well the location and orientation of the anchor, $\boldsymbol{r}(0,t_0)$, $\boldsymbol{X}(0,t_0)$, $\boldsymbol{Y}(0,t_0)$ and $\boldsymbol{Z}(0,t_0)$. The centre line curve $\boldsymbol{r}(s,t_0)$ can be reconstructed by integrating

$$\boldsymbol{r}(s,t_0) = \boldsymbol{r}(0,t_0) + \int_0^s \boldsymbol{Z}(\xi,t_0)\mathrm{d}\xi, \quad (6)$$

and the body coordinate system $\boldsymbol{X}(s,t_0)$, $\boldsymbol{Y}(s,t_0)$, $\boldsymbol{Z}(s,t_0)$ is obtained by integrating

$$\boldsymbol{X}_s = \kappa_Z\boldsymbol{Y} - \kappa_Y\boldsymbol{Z}, \quad (7)$$

$$\boldsymbol{Y}_s = -\kappa_Z\boldsymbol{X} + \kappa_X\boldsymbol{Z}, \quad (8)$$

$$\boldsymbol{Z}_s = \kappa_Y\boldsymbol{X} - \kappa_X\boldsymbol{Y} \quad (9)$$

with respect to s.

(ii) *Relating the drag force exerted by the surrounding fluid to the local velocity*

The hydrodynamic description we use here was developed by Gueron & Liron (1992). It accounts for 3D flow fields and enables simulations of multicilia configurations while taking the hydrodynamic interactions into account. This relationship in body coordinates is

$$\phi_X = -C_X V_X + g_X, \quad (10)$$

$$\phi_Y = -C_Y V_Y + g_Y \quad (11)$$

and

$$\phi_Z = -C_Z V_Z + g_Z, \quad (12)$$

where $\boldsymbol{\phi}(s,t)$ is the drag force per unit length exerted by the cilium on the surrounding fluid of viscosity μ, $g_X = C_X G_X$, $g_Y = C_Y G_Y$ and $g_Z = C_Z G_Z$ and $\boldsymbol{G} = (G_X, G_Y, G_Z)$ denotes the velocity field induced at s by 'far segments' of the cilium, neighbouring cilia or external flow. The components of $\boldsymbol{G}$ are expressed in terms of singular solutions of Stokes' equations. The tangential (C_Z) and normal (C_X, C_Y) resistance coefficients are

$$C_Z = \frac{8\pi\mu}{-2 + 4\ln(2q/a)} \quad (13)$$

and

$$C_X = C_Y = \frac{8\pi\mu}{1 + 2\ln(2q/a)} \quad (14)$$

for any q such that $a \ll q$ and $q \ll 1$. These are *not* the Gray–Hancock resistance coefficients and their ratio $C_N/C_T \approx 1.43$ is lower than the value 2 used in the Gray–Hancock approximation (detailed discussion is given in Gueron & Liron (1992) and Gueron & Levit-Gurevich (1998)). The expression for $\boldsymbol{G}$ is

$$\begin{aligned}\boldsymbol{G}(s_0,t) = {} & \int_{|s-s_0|>q} \boldsymbol{U}_s(\boldsymbol{r}(s_0,t), \boldsymbol{r}(s,t)), -\boldsymbol{\phi}(s,t))\mathrm{d}s \\ & + \int_{0\leqslant s\leqslant 1} \{\boldsymbol{V}_{\text{si}}(\boldsymbol{r}(s_0,t), \boldsymbol{r}(s,t)), -\boldsymbol{\phi}(s,t)) \\ & + \boldsymbol{V}_{\text{di}}(\boldsymbol{r}(s_0,t), \boldsymbol{r}(s,t), -(a^2/4\mu)\boldsymbol{\phi}(s,t))\}\mathrm{d}s \\ & + \int_{\substack{0\leqslant s\leqslant 1 \\ \text{neighbouring cilia}}} \boldsymbol{U}_s(\boldsymbol{r}(s_0,t), \boldsymbol{r}(s,t), -\boldsymbol{\phi}(s,t))\mathrm{d}s,\end{aligned} \quad (15)$$

where $\boldsymbol{U}_s(\boldsymbol{r}, \boldsymbol{r}_0, \boldsymbol{\phi})$ is the velocity induced at $\boldsymbol{r}$ by a Stokeslet with intensity $\boldsymbol{\phi}$ located at $\boldsymbol{r}_0$, $\boldsymbol{V}_{\text{si}}(\boldsymbol{r}, \boldsymbol{r}_0, \boldsymbol{\phi})$ is the velocity induced by the image system of the Stokeslet alone and $\boldsymbol{V}_{\text{di}}$ is the velocity induced by the image system of the doublet alone.

The mechanical equilibrium at which the cilium is found implies the balance $\boldsymbol{F}_s = \boldsymbol{\phi}$ which reads, by components,

$$\phi_X = F_{X_s} - \kappa_Z F_Y + \kappa_Y F_Z, \quad (16)$$

$$\phi_Y = F_{Y_s} + \kappa_Z F_X - \kappa_X F_Z \quad (17)$$

and

$$\phi_{\mathcal{Z}} = F_{\mathcal{Z}_s} - \kappa_{\mathcal{Y}} F_X + \kappa_X F_{\mathcal{Y}}. \tag{18}$$

From equations (10)–(12) and (16)–(18) we rewrite equation (5) as

$$\begin{aligned} F_{\mathcal{Z}_{ss}} = {} & (1 + C_{\mathcal{Z}X})\kappa_{\mathcal{Y}} F_{X_s} + C_{\mathcal{Z}X}(\kappa_X^2 + \kappa_{\mathcal{Y}}^2) + F_{\mathcal{Z}}\kappa_{\mathcal{Y}_s} F_X \\ & - \kappa_{X_s} F_{\mathcal{Y}} - (1 + C_{\mathcal{Z}X})\kappa_X F_{\mathcal{Y}_s} - C_{\mathcal{Z}X}[\kappa_{\mathcal{Y}} F_{\mathcal{Y}} + \kappa_X F_X]\kappa_{\mathcal{Z}} \\ & + C_{\mathcal{Z}X}[K_X g_{\mathcal{Y}} - \kappa_{\mathcal{Y}} g_X] + g_{\mathcal{Z}_s}, \end{aligned} \tag{19}$$

where $C_{\mathcal{Z}X} = C_{\mathcal{Z}}/C_X$.

The components of the internal shear force in the X and $\mathcal{Y}$ directions are modelled as the sum of elastic and active shear forces. Using the balance of moments ($\boldsymbol{M}_s = \boldsymbol{Z} \times \boldsymbol{F}$) and the assumption that the filaments are linearly elastic, we model the internal shear forces by

$$F_X = E_B \kappa_{\mathcal{Y}_s} + (E_B - E_T)\kappa_X \kappa_{\mathcal{Z}} + S, \tag{20}$$

$$F_{\mathcal{Y}} = -E_B \kappa_{X_s} + (E_B - E_T)\kappa_{\mathcal{Y}} \kappa_{\mathcal{Z}} + P. \tag{21}$$

Here, E_B and E_T are the bending and twisting resistance coefficients and $S = S(s, t)$ and $P = P(s, t)$ represent the respective components of the shear force. The angular velocity is related to the active mechanism by (Gueron & Levit-Gurevich 2000)

$$C_\Omega \Omega(s, t) = E_T \kappa_{\mathcal{Z}_s}(s, t) + R(s, t), \tag{22}$$

where $C_\Omega = 4\pi\mu a^2$ is the rotation resistance coefficient and R denotes the active twisting moment per unit length.

(iii) *A new model for the 9 + 2 internal mechanism*

Our new three-state 'ready–duty–rest' model for the reactivation process of the dynein arms by ATP molecules that diffuse through the cilium is described below.

3. MODELLING THE CILIARY INTERNAL MECHANISM: MECHANICAL CONSIDERATION

Let $\boldsymbol{M}_a(s)$ be the moment induced by the active system at the centre line point s and let $\boldsymbol{M}_i(s)$ be the portion of the moment due to filament i (we use a cyclic modulo 9 notation for the index i). The force per unit length contributed by filament i is denoted by $\boldsymbol{f}_{d_i}(s)$ and the total force due to filament i is therefore

$$\boldsymbol{F}_{d_i}(s) = -\int_s^l \boldsymbol{f}_{d_i}(\xi)\mathrm{d}\xi. \tag{23}$$

Our goal here is to reduce the ciliary motion modelling problem to determining model equations for $\boldsymbol{f}_{d_i}$, which are derived in § 4.

We denote the vector connecting the centre line with the ith doublet or filament by $\boldsymbol{L}_i(s)$, where

$$\boldsymbol{L}_i(s) = a\left[\cos\left(\frac{2\pi}{9}(1-i)\right)\boldsymbol{X}(s) + \sin\left(\frac{2\pi}{9}(1-i)\right)\boldsymbol{Y}(s)\right], \tag{24}$$

and define $\boldsymbol{e}_i(s)$ and $\boldsymbol{b}_i(s)$ by

$$\boldsymbol{e}_i(s) = \boldsymbol{L}_{i+1}(s) - \boldsymbol{L}_i(s), \tag{25}$$

$$\boldsymbol{b}_i(s) = \boldsymbol{e}_i(s) \times \boldsymbol{Z}(s). \tag{26}$$

An illustration is presented in figure 1*d*.

In order to model the active shear forces, the bending and twisting moments, we consider three types of links between the filaments: dynein cross-bridges, radial spokes and nexin links. The dynein arms undergo a periodic mechanochemical process of attachment–detachment and are classified as an active component of the system (Sleigh & Barlow 1982; Hines & Blum 1983; Satir 1994). The nexin links connect two adjacent doublets in a permanent link and may be considered to be playing a passive role, contributing to the axoneme's bending resistance (Hines & Blum 1983). The role of the radial spokes is not completely clear, in particular whether they are to be considered as an active or passive component (see Sleigh & Barlow 1982; Hines & Blum 1983; Satir 1994). Here we use our model to suggest that the radial spokes must actively contribute to the twist along the cilium. To that end, suppose that the dynein cross-bridges are the only active part of the internal mechanism. As filament i is influenced by filaments $i-1$ and i itself (see figure 1*e*), we write

$$\boldsymbol{M}_i(s) = -\boldsymbol{L}_i(s) \times \int_s^l [\boldsymbol{f}_{d_i}(\xi) - \boldsymbol{f}_{d_{i-1}}(\xi)]\mathrm{d}\xi. \tag{27}$$

Therefore, the total moment due to the dynein arms is

$$\begin{aligned} \boldsymbol{M}_a(s) = \sum_{i=1}^{9} M_{a_i}(s) &= \sum_{i=1}^{9} \boldsymbol{L}_i(s) \times (\boldsymbol{F}_{d_i}(s) - \boldsymbol{F}_{d_{i-1}}(s)) \\ &= -\sum_{i=1}^{9} \boldsymbol{e}_i(s) \times \boldsymbol{F}_{d_i}(s). \end{aligned} \tag{28}$$

Relating the shear force to the active moment (via balance of moments), we obtain

$$\begin{aligned} \boldsymbol{S} = \frac{\partial \boldsymbol{M}_a}{\partial s} = \boldsymbol{\kappa} \sum_{i=1}^{9} (\boldsymbol{e}_i \times \boldsymbol{F}_{d_i}) - \sum_{i=1}^{9} (\boldsymbol{\kappa} \times \boldsymbol{F}_{d_i}) \\ \times \boldsymbol{e}_i - \sum_{i=1}^{9} \boldsymbol{e}_i \times \boldsymbol{f}_{d_i}. \end{aligned} \tag{29}$$

(a) *Conclusion*

From equation (29) we can see that, if $\kappa_{\mathcal{Z}} \neq 0$, then the $\mathcal{Z}$ component of the shear force $\boldsymbol{M}_{a_s} \times \boldsymbol{Z} = \kappa_{\mathcal{Z}} \sum_{i=1}^{9} \boldsymbol{e}_i \times \boldsymbol{F}_{d_i}$, *does not vanish*, as it is supposed to, by mechanical equilibrium. Therefore, there must be another active system, in addition to the dynein arms, which balances the twist occurring in the X–$\mathcal{Y}$ plane, in order to prevent distortion of the axoneme and to keep the cross-section circular. This motivates our speculation that the twist resistance is at least partly due to the radial spokes system. Denoting the active moment due to the dynein arms by $\boldsymbol{M}_d$ and the active moment due to the radial spokes by $\boldsymbol{M}_r$, we write

$$\begin{aligned} \boldsymbol{M}_a &= \boldsymbol{M}_d + \boldsymbol{M}_r = M_{d_X}\boldsymbol{X} + M_{d_{\mathcal{Y}}}\boldsymbol{Y} + M_{d_{\mathcal{Z}}}\boldsymbol{Z} + M_r\boldsymbol{Z} \\ &= M_X\boldsymbol{X} + M_{\mathcal{Y}}\boldsymbol{Y} + M_{\mathcal{Z}}\boldsymbol{Z}, \end{aligned} \tag{30}$$

where (from equation (28))

$$M_X = M_{d_X} = -\sum_{i=1}^{9} (\boldsymbol{e}_i(s) \times \boldsymbol{F}_{d_i}(s)) \times \boldsymbol{X}, \tag{31}$$

$$M_Y = M_{d_Y} = -\sum_{i=1}^{9} (\boldsymbol{e}_i(s) \times \boldsymbol{F}_{d_i}(s)) \times \boldsymbol{Y}, \tag{32}$$

$$M_Z = M_{d_Z} + M_r. \tag{33}$$

Differentiating $\boldsymbol{M}_a$ with respect to s gives

$$\begin{aligned}\boldsymbol{M}_{a_s} = {} & (M_{X_s} - \kappa_Z M_Y + \kappa_Y M_Z)\boldsymbol{X} \\ & + (M_{Y_s} + \kappa_Z M_X - K_X M_Z)\boldsymbol{Y} \\ & + (M_{Z_s} - \kappa_Y M_X + K_X M_Y)\boldsymbol{Z},\end{aligned} \tag{34}$$

and by using $\boldsymbol{M}_{a_s} \times \boldsymbol{Z} = \boldsymbol{0}$ we obtain

$$M_{Z_s} - \kappa_Y M_X + \kappa_X M_Y = 0. \tag{35}$$

On the other hand,

$$\begin{aligned}M_{Z_s} &= M_{d_{Z_s}} + M_{r_s} = (\boldsymbol{M}_d \times \boldsymbol{Z})_s + M_{r_s} \\ &= (\boldsymbol{M}_{d_s} \times \boldsymbol{Z}) + (\boldsymbol{M}_d \times \boldsymbol{Z}_s) + M_{r_s} \\ &= \kappa_Z \sum_{i=1}^{9} (\boldsymbol{e}_i \times \boldsymbol{F}_{d_i}) + \kappa_Y M_X - \kappa_X M_Y + M_{r_s},\end{aligned} \tag{36}$$

and, therefore,

$$M_r(s) = \int_s^l \kappa_Z(\xi) \sum_{i=1}^{9} (\boldsymbol{e}_i(\xi) \times \boldsymbol{F}_{d_i}(\xi))\mathrm{d}\xi. \tag{37}$$

This implies that the radial spokes contribute to the twisting moment only when the cilium is out of plane, i.e. when $\kappa_Z \neq 0$. Combining equations (28), (33) and (37) and using equation (26) we obtain

$$\begin{aligned}M_Z(s) = {} & \sum_{i=1}^{9} (\boldsymbol{b}_i(s) \times \boldsymbol{F}_{d_i}(s)) + \int_s^l \kappa_Z(\xi) \sum_{i=1}^{9} (\boldsymbol{e}_i(\xi) \\ & \times \boldsymbol{F}_{d_i}(\xi))\mathrm{d}\xi.\end{aligned} \tag{38}$$

We now denote the X and Y components of the active shear forces by $S(s, t)$ and $P(s, t)$, respectively, and denote the active twisting moment per unit of length by $R(s, t)$. This leads to the following model equations for the internal ciliary engine:

$$S(s, t) = \boldsymbol{M}_{a_s} \times \boldsymbol{Y} = M_{Y_s} + \kappa_Z M_X - \kappa_X M_Z, \tag{39}$$

$$P(s, t) = -\boldsymbol{M}_{a_s} \times \boldsymbol{X} = -M_{X_s} + \kappa_Z M_Y - \kappa_Y M_Z, \tag{40}$$

$$R(s, t) = (\boldsymbol{M}_a \times \boldsymbol{Z})_s = \kappa_Y M_X - \kappa_X M_Y. \tag{41}$$

4. MODELLING DYNEIN ARMS' MECHANOCHEMICAL CYCLE

We now use equations (31), (32) and (38)–(41) to relate the active shear forces and the bending and twisting moments to $\boldsymbol{f}_{d_i}$. We first note that, knowing which dynein arms are active at a given instance, we can compute the components of the moments from equations (31), (32) and (38) and then compute the active shear forces and twisting moment per unit length by using equations (39)–(41). We now assume that each dynein arm is found at one of the following three states (see Satir 1994).

(i) *The duty phase*, where the arm is reactivated by an ATP molecule and attaches to the adjacent doublet. The duration of this phase is denoted by τ_{duty}.
(ii) *The rest phase*, which follows the duty phase, is a period of duration τ_{rest} before the dynein arm can be reactivated.
(iii) *The ready phase* is the state before the next duty phase, where the dynein arm is ready to hydrolyse an ATP molecule.

The dynein arm can therefore start a new reactivation cycle only after a time-interval $\tau_{\mathrm{cycle}} = \tau_{\mathrm{duty}} + \tau_{\mathrm{rest}}$. We assume here that the dynein arms are distributed uniformly along the filaments and denote the number of dynein arms per unit length by $\mathcal{N} = 2l/(d \times l) = 2/d$ where l is a cilium's length, d is the distance between two adjacent dynein pairs and the factor 2 accounts for the outer and inner arms (note that the inner and outer dynein arms have different functions (see Brokaw 1999), but for simplicity we are treating them as if they were identical for the purpose of this model).

We denote the numbers of dynein arms per unit length along the ith filament found at the duty, ready and rest states by $\mathcal{N}_{\mathrm{duty}_i}(s, t)$, $\mathcal{N}_{\mathrm{ready}_i}(s, t)$ and $\mathcal{N}_{\mathrm{rest}_i}(s, t)$, respectively, having $\mathcal{N}_{\mathrm{duty}_i}(s, t) + \mathcal{N}_{\mathrm{ready}_i}(s, t) + \mathcal{N}_{\mathrm{rest}_i}(s, t) = \mathcal{N}$. The active force per unit length contributed by the activated dynein arms along the ith filament can be modelled by (see figure 1*d*,*e*)

$$\boldsymbol{f}_{d_i}(s) = \frac{\sqrt{2}}{2} S_0 \mathcal{N}_{\mathrm{duty}_i}(s) \left[\frac{1}{\|\boldsymbol{e}_i\|}\boldsymbol{e}_i(s) - \boldsymbol{Z}(s)\right], \tag{42}$$

where S_0 is the magnitude of the force due to a single arm. In order to model $\mathcal{N}_{\mathrm{duty}_i}$, we denote the reactivation rate of the ready dynein arms by $\mathcal{N}_{\mathrm{ready}\to\mathrm{duty}_i}(s, t)$ and propose

$$\begin{cases}\dot{\mathcal{N}}_{\mathrm{duty}_i}(s, t) &= \mathcal{N}_{\mathrm{ready}\to\mathrm{duty}_i}(s, t) - \mathcal{N}_{\mathrm{ready}\to\mathrm{duty}_i}(s, t - \tau_d) \\ \dot{\mathcal{N}}_{\mathrm{rest}_i}(s, t) &= \mathcal{N}_{\mathrm{ready}\to\mathrm{duty}_i}(s, t - \tau_d) - \mathcal{N}_{\mathrm{ready}\to\mathrm{duty}_i}(s, t - \tau_d) \\ \dot{\mathcal{N}}_{\mathrm{ready}_i}(s, t) &= \mathcal{N}_{\mathrm{ready}\to\mathrm{duty}_i}(s, t - \tau_c) - \mathcal{N}_{\mathrm{ready}\to\mathrm{duty}_i}(s, t),\end{cases} \tag{43}$$

where $\mathcal{N}_{\mathrm{ready}\to\mathrm{duty}_i}$ is modelled by

$$\mathcal{N}_{\mathrm{ready}\to\mathrm{duty}_i}(s, t) = kc(s, t)\mathcal{N}_{\mathrm{ready}_i}(s, t). \tag{44}$$

Here, $c(s, t)$ denotes the local ATP concentration and $k = k_0 \times P(s) = k_0(1 - s^2)$, where k_0 is a parameter and P is the reactivation probability in the presence of an ATP molecule near a ready dynein arm. To account for the diffusion of ATP from the cell body throughout the cilium (see Raff & Blum 1968), we write (using equation (44))

$$\begin{aligned}\frac{\partial c(s, t)}{\partial t} &= -\sum_{i=1}^{9} \mathcal{N}_{\mathrm{ready}\to\mathrm{duty}_i}(s, t) + D\frac{\partial^2 c(s, t)}{\partial s^2} \\ &= -kc(s, t)\sum_{i=1}^{9} \mathcal{N}_{\mathrm{ready}_i}(s, t) + D\frac{\partial^2 c(s, t)}{\partial s^2},\end{aligned} \tag{45}$$

where D denotes the diffusion coefficient.

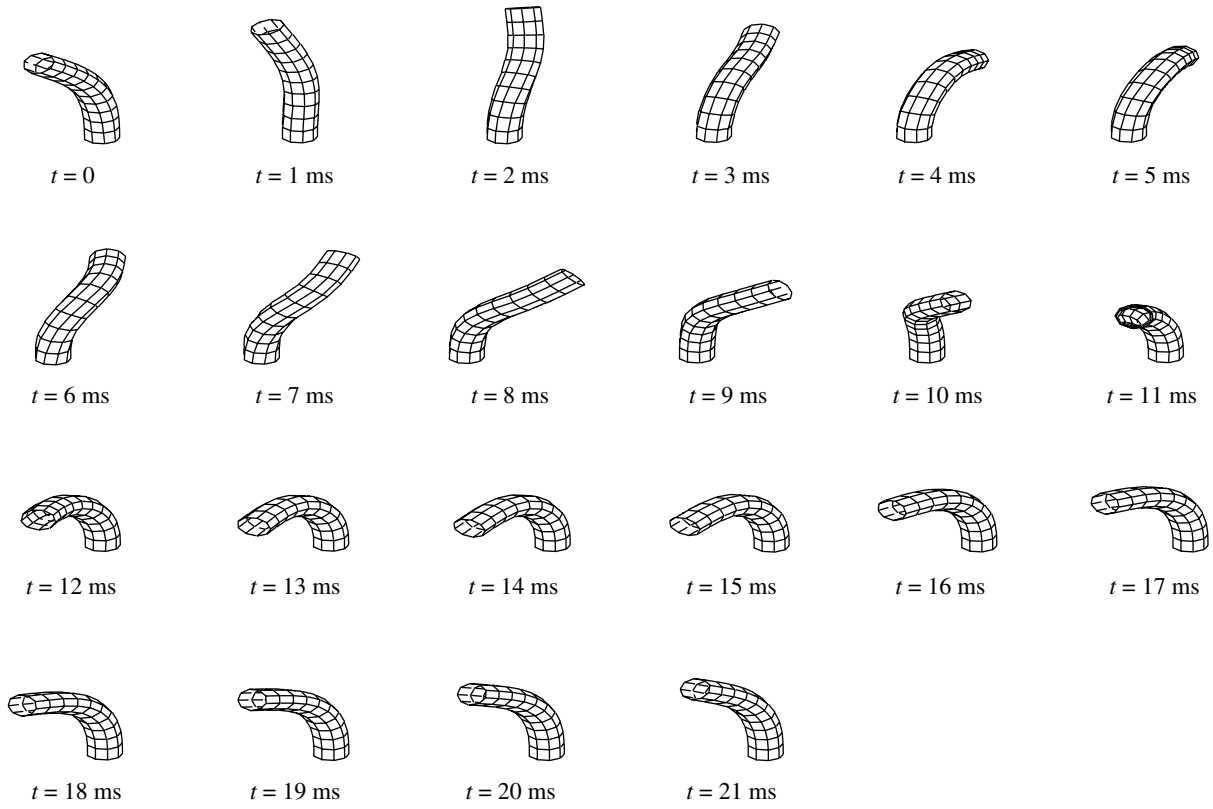

Figure 2. A single model cilium beating in water. A 'wire frame' display.

5. BOUNDARY CONDITIONS AND CHOICE OF PARAMETERS

(a) *Boundary conditions*

The model cilium is free at its distal end and clamped rigidly in an erect position at the anchor. At the free end all forces and moments vanish and we can write

$$\boldsymbol{F}(1,t)=0, \tag{46}$$

$$S(1,t)=P(1,t)=0 \tag{47}$$

and

$$\kappa_X(1,t)=\kappa_Y(1,t)=\kappa_Z(1,t)=0. \tag{48}$$

At the basal end we have

$$\kappa_X(0,t)=\kappa_Y(0,t)=0, \tag{49}$$

$$\kappa_Z(0,t)=0, \tag{50}$$

$$\boldsymbol{V}(0,t)=\boldsymbol{V}_s(0,t)=\boldsymbol{\phi}(0,t)=\boldsymbol{\phi}_s(0,t)=0 \tag{51}$$

and

$$\boldsymbol{\Omega}(0,t)=0. \tag{52}$$

The body coordinate system at the anchor is stationary:

$$\boldsymbol{X}_t(0,t)=0, \tag{53}$$

$$\boldsymbol{Y}_t(0,t)=0 \tag{54}$$

and

$$\boldsymbol{Z}_t(0,t)=0, \tag{55}$$

and we therefore have $\omega_Z(0,t)=0$.

We assume that the concentration of ATP at the basal end is fixed and it does not change at the distal end:

$$c(0,t)=c_0 \tag{56}$$

and

$$\frac{\partial c(1,t)}{\partial s}=0. \tag{57}$$

No dynein arms at the ciliary base (see Murase 1992) lead to

$$\begin{aligned}\mathcal{N}_{\mathrm{ready}_i}(0,t)=\mathcal{N}_{\mathrm{duty}_i}(0,t)&=\frac{\partial \mathcal{N}_{\mathrm{ready}_i}(0,t)}{\partial s}\\ &=\frac{\partial \mathcal{N}_{\mathrm{duty}_i}(0,t)}{\partial s}=0, \quad 1\leqslant i\leqslant 9\end{aligned} \tag{58}$$

The initial conditions we use here are

$$c(s,0)=c_0, \tag{59}$$

$$\mathcal{N}_{\mathrm{ready}_i}(s,0)=1 \tag{60}$$

and

$$\mathcal{N}_{\mathrm{duty}_i}(s,0)=0, \qquad 1\leqslant i\leqslant 4, \tag{61}$$

and $\mathcal{N}_{\mathrm{ready}_i}(s,0)=\mathcal{N}_{\mathrm{duty}_i}(s,0)=0$ for the rest filaments.

For complete details of the numerical procedure see Gueron & Levit-Gurevich (2000).

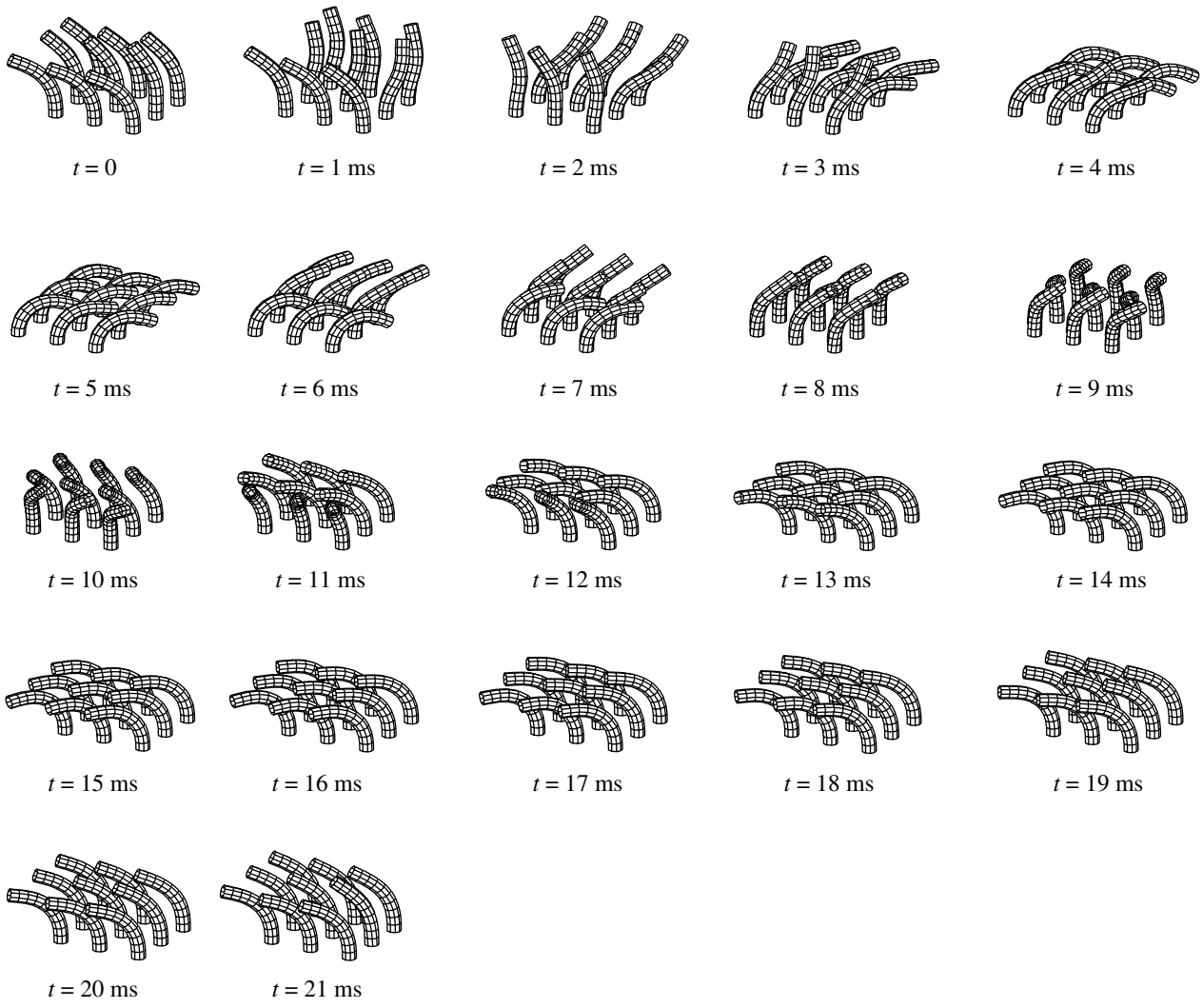

Figure 3. The beat of a 3 × 3 ciliary array. The interciliary distance in both directions is half a ciliary length.

(b) *Choice of parameters*

In our simulations we used the following parameters: $l = 10^{-5}$ m (a cilium's length), $q = 10^{-6}$ m, $a = 10^{-7}$ m, $E_B = E_T = 25 \times 10^{-24}$ kg m^3 s^{-2}, $\mu = 0.001$ kg m^{-1} s^{-1}, $w = 25$ Hz, $S_0 = 10^{-12}$N−typical shear force. In non-dimensional form, these yield $C_X = 0.01438$, $C_Z = 0.01$ and $C_\Omega = 0.00314$. These parameters are suitable for the cilium of *Paramecium* beating in water (see Gueron & Liron 1992). In our numerical implementation we used $N = 100$ discretization points along the curve and the time-step $\mathrm{d}t = 0.0001$ s.

For the engine equations the parameters were chosen in the following manner: $d = 24$ nm, $\tau_e = 33$ ms and $\tau_d = 3$ ms (see Satir 1994). The ATP concentration at the base is $c_0 = 0.3$ mM $= 5.68 \times 10^9$ molecule m^{-1} (see Brokaw 1975). The coefficient in the calculation of the translation rate from ready state to duty state is $k_0 = 200$ m s^{-1}. The diffusion coefficient is chosen to be $D = 0.3 \times 10^{-8}$ m^2 s^{-1}.

6. RESULTS

Figure 2 shows diagrams of the beat cycle of an isolated model cilium beating in water. The cilium is illustrated with its nine doublets and nexin links 'skeleton' (the radius is not to scale). The resulting beat duration and beat frequency are 22 ms and 45 Hz, respectively.

Our 3D model was used for checking the effect of increased viscosity which, as expected, changed the beat pattern and frequency. The new feature of the model is that the cilium autonomously changes its effective stroke plane. For example, when the viscosity was set to ten times that of water, the effective stroke plane rotated by $\approx 12^\circ$ with respect to the plane of the effective stroke at the viscosity of water (simulations not shown). Such capability in changing the plane of beating is important for ciliary function and was indeed observed by Machemer (1972). It also indicates a possible source for different types of metachronal coordination other than anti-plectic metachronal patterns (Sleigh 1962; Machemer 1972; Murase 1992) which occur in rows of cilia having a planar beat (Gueron & Levit-Gurevich 1998).

Figure 3 displays diagrams of the beat pattern of a 3 × 3 rectangular ciliary array. Although the model cilia are identical and are started with the same initial conditions, phase shifts evolve autonomously due to the hydrodynamical coupling. Figure 4 shows displays diagrams of the beat pattern of a 5 × 5 rectangular ciliary array. The top lines show diagrams of the cilia. The bottom lines illustrate the 'waveform sheet' that is

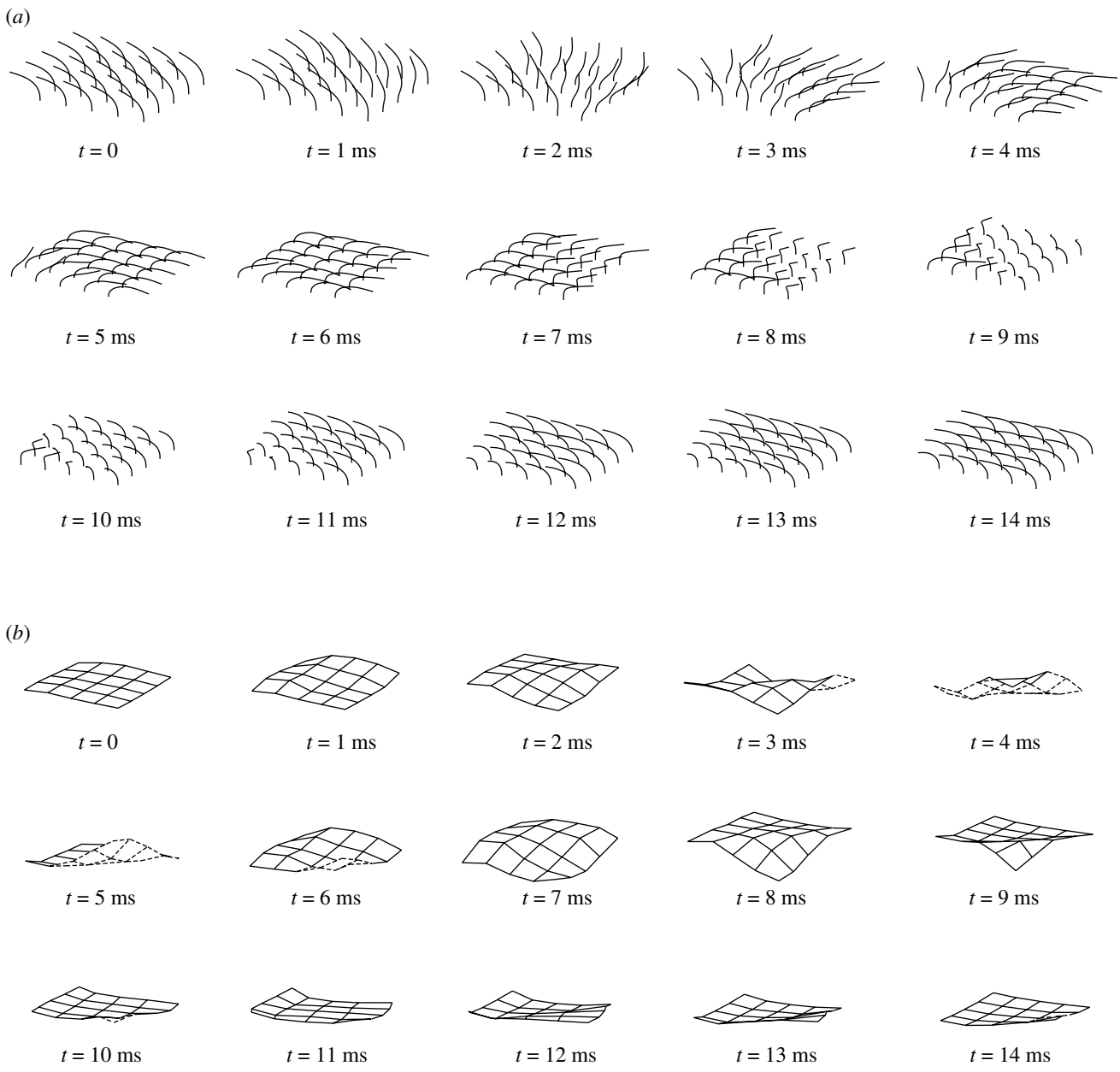

Figure 4. The beat of a 5×5 ciliary array. The interciliary distance in both directions is half a ciliary length. (*a*) 3D view of the array. (*b*) The sheet formed by the tips of the beating cilia at the same time.

formed by the tips of the cilia, which resembles a metachronal pattern.

7. DISCUSSION

Our modelling platform first allows simulations of 3D motion of multicilia arrays at a detailed level related directly to the internal structure. Here we have only treated cilia having a $9 + 2$ internal structure, trying to speculate on the role of the radial spokes. Our model for the internal engine is a simplified approach. It is based on knowing the state and geometric positions of the dynein arms without presuming additional details concerning the behaviour of the radial spokes and the nexin links. However, other structures such as $12 + 0$, $9 + 0$ and $6 + 0$, which have no central pair and perhaps no radial spokes, also exist. These need to be treated differently. Our internal engine model is, to our knowledge, the first that accounts for the dynein kinetics in such a detailed manner. Nevertheless, due to the absence of a more detailed biological description of the processes experienced by real dynein (e.g. the distortion of the dynein molecule), we avoid incorporating comprehensive mechanochemical details and, thus, use a simplified model. Further modelling work is still needed to extend the model.

In order to tackle the 3D geometrical problem, we approximated the cilium as an elastic cylinder that maintains a fixed planar and circular cross-section. This assumption may be too crude since initially planar cross-sections experience distortions during motion. A geometric model that takes these distortions into account is our next challenge.

We hope that the proposed modelling platform will help experimenters and theoreticians increase their understanding of the puzzle of ciliary beating.

We thank Professor Jacob J. Blum from the Duke University Medical Center for helpful discussions, help and suggestions for improving the presentation. This research was supported by the US–Israel Binational Science Foundation (grant number 97-00400) and by a grant from the Israeli Ministry of Science. K.L.-G. acknowledges the support of the Technion Graduate School and the Selim and Rachel Benin Fund, The United Jewish Appeal Federation, New York.

REFERENCES

Brokaw, C. J. 1975 Effects of viscosity and ATP concentration on the movement of reactivated sea-urchin sperm flagella. *J. Exp. Biol.* **62**, 701–719.

Brokaw, C. J. 1999 Computer simulation of flagellar movement. VII. Conventional but functionally different cross-bridge models for inner and outer arm dyneins can explain the effects of outer arm dynein removal. *Cell Motil. Cytoskel.* **42**, 134–148.

Gheber, L. & Priel, Z. 1989 Synchronization between beating cilia. *Biophys. J.* **55**, 183–191.

Gueron, S. & Levit-Gurevich, K. 1998 Computation of the internal forces in cilia: application to ciliary motion, the effects of viscosity and cilia interactions. *Biophys. J.* **74**, 1658–1676.

Gueron, S. & Levit-Gurevich, K. 1999 Energetic considerations of ciliary beating and the advantage of metachronal coordination. *Proc. Natl Acad. Sci. USA* **96**, 12 240–12 245.

Gueron, S. & Levit-Gurevich, K. 2000 The three dimensional motion of slender filaments. *Math. Methods Appl. Sci.* (In the press.)

Gueron, S. & Liron, N. 1992 Ciliary motion modeling and dynamic multicilia interactions. *Biophys. J.* **63**, 1045–1058.

Gueron, S. & Liron, N. 1993 Simulations of three-dimensional ciliary beats and cilia interactions. *Biophys. J.* **65**, 499–507.

Gueron, S., Levit-Gurevich, K., Liron, N. & Blum, J. J. 1997 Cilia internal mechanism and metachronal coordination as the result of hydrodynamical coupling. *Proc. Natl Acad. Sci. USA* **94**, 6001–6006.

Hines, M. & Blum, J. J. 1978 Bend propagation in flagella. I. Derivation of equations of motion and their simulation. *Biophys. J.* **23**, 41–57.

Hines, M. & Blum, J. J. 1983 Three-dimensional mechanics of eukaryotic flagella. *Biophys. J.* **41**, 67–79.

Machemer, H. 1972 Ciliary activity and the origin of metachronism in paramecium: effects of increased viscosity. *J. Exp. Biol.* **57**, 239–259.

Mogami, Y., Pernberg, J. & Machemer, H. 1992 Ciliary beating in three dimensions: steps of quantitative description. *J. Math. Biol.* **30**, 215–249.

Murase, M. 1992 *Dynamics of cellular motility.* New York: John Wiley & Sons Ltd.

Raff, E. C. & Blum, J. J. 1968 A possible role for adenylate kinase in cilia: concentration profiles in a geometrically constrained dual enzyme system. *J. Theor. Biol.* **18**, 53–71.

Satir, P. 1994 Biochemical events in the production of ciliary movement. In *Biomechanics of active movement and division of cells* (ed. N. Akkas), pp. 465–470.

Sleigh, M. A. 1962 *The biology of cilia and flagella.* Oxford, UK: Pergamon Press.

Sleigh, M. A. (ed.) 1974 *Cilia and flagella.* London: Academic Press.

Sleigh, M. A. & Barlow, D. I. 1982 How are different ciliary beat patterns produced? *Symp. Soc. Exp. Biol.* **35**, 139–157.

Sugino, K. & Machemer, H. 1987 Axial-view recording: an approach to assess the third dimension of the ciliary cycle. *J. Theor. Biol.* **125**, 67–82.

Sugino, K. & Machemer, H. 1988 The ciliary cycle during hyperpolarization-induced activity: an analysis of axonemal functional parameters. *Cell Motil. Cytoskel.* **11**, 275–290.

Teunis, P. F. M. & Machemer, H. 1994 Analysis of three dimensional ciliary beating by means of high-speed stereomicroscopy. *Biophys. J.* **67**, 381–394.

Wooley, D. M. & Vernon, G. G. 1999 Alternating torsions in a living '9+2' flagellum. *Proc. R. Soc. Lond.* B **266**, 1271–1275.

As this paper exceeds the maximum length normally permitted, the authors have agreed to contribute to production costs.